CHEMICAL ENGINEERING TRANSACTIONS
VOL. 35, 2013
A publication of AIDIC
The Italian Association of Chemical Engineering
www.aidic.it/cet
Guest Editors: Petar Varbanov, Jiří Klemeš, Panos Seferlis, Athanasios I. Papadopoulos, Spyros Voutetakis

ISBN 978-88-95608-26-6; **ISSN** 1974-9791
DOI: 10.3303/CET1335018

Modelling and Simulation of a Membrane Reactor for the Low Temperature Methane Steam Reforming

Alexios-Spyridon Kyriakides[a,b], Dimitris Ipsakis[a], Spyros Voutetakis[a,*], Simira Papadopoulou[a,c], Panos Seferlis[a,b]

[a]Chemical Process & Energy Resources Institute (C.P.E.R.I.), Center for Research and Technology Hellas (CE.R.T.H.), P.O. Box 60361, 57001, Thermi-Thessaloniki, Greece
[b]Department of Mechanical Engineering, Aristotle University of Thessaloniki, P.O. Box 484, 54124 Thessaloniki, Greece
[c]Automation Department, Alexander Technological Educational Institute of Thessaloniki, P.O. Box 141, 57400 Thessaloniki, Greece
Spyros Voutetakis paris@cperi.certh.gr

In the present study, a two-dimensional (2D), nonlinear, and pseudo-homogeneous mathematical model of a fixed-bed catalytic reactor with an integrated membrane for the methane steam reforming over a nickel-based catalyst is developed. A permselective Pd based membrane is used in order to remove hydrogen from the reaction zone and shift the equilibrium towards hydrogen production thus enabling the achievement of a high methane conversion. The nickel-based catalyst allows for significantly low operating temperatures (less than 550 ^{o}C) than conventional methane reforming. The necessary heat for the initiation and preservation of the reactions is supplied to the reactor through an external source. The mathematical model is based on rigorous mass, energy, and momentum balances, where both axial and radial gradients of mass and temperature are fully considered. Hydrogen flux through the membrane is calculated by Sieverts law where the driving force is the hydrogen partial pressure difference between the two sides of the membrane. Results referring to the distribution of species and methane conversion along the reactor and temperature and hydrogen flowrate along the reactor for different radial positions are obtained and analyzed. Furthermore, sensitivity analysis on the effect of different wall temperatures (500 ^{o}C, and 550 ^{o}C) and operating pressures (1, 5, and 10 atm) show that in a membrane reactor methane conversion (60.24 % at 10 atm) can reach similar values to that in a traditional reactor (61.21 % at 10 atm and 700^{o}C) at significantly lower temperatures (550 ^{o}C).

1. Introduction

Methane steam reforming (MSR) for hydrogen production is a promising process, but is limited by thermodynamic equilibrium, since reactions has to take place at high temperatures (>800 ^{o}C) in order to reach significantly high methane conversion and thus, high hydrogen yield. Similar or even higher methane conversion can be achieved in membrane reactors at much lower temperatures (less than 550 ^{o}C), where hydrogen is removed from the reactive zone through a permselective Pd or Pd-Ag based membrane. As a result, thermodynamic equilibrium shifts towards hydrogen production due to effective pressure differences (Bientinesi and Petarca, 2011). Hydrogen is then carried away by a sweep gas, commonly a stream of H_2O, N_2 or He. A major advantage of such process is that the hydrogen stream becomes free of CO and CO_2, which makes it suitable for fuel cell and other power production applications. Another benefit of membrane reactors for MSR is that water gas shift reaction is favoured at lower temperatures and CO concentrations in the effluent stream can be significantly lowered (De Falco et al., 2011b).
Reforming reactor using Pd membranes have been studied experimentally in a number of configurations by De Falco et al. (2011a). Specifically, the option of embedded or external membrane configurations was investigated. The use of solar heated molten salts as an external source of thermal energy enables the enhancement of process sustainability (De Falco et al., 2008). In a similar study (Simakov and Sheintuch,

Please cite this article as: Kyriakides A.S., Ipsakis D., Voutetakis S., Papadopoulou S., Seferlis P., 2013, Modeling and simulation of a membrane reactor for the low temperature methane steam reforming, Chemical Engineering Transactions, 35, 109-114 DOI:10.3303/CET1335018

2010), it was shown that the presence of a recycle gas oven, significantly improves the thermal efficiency of the process. A two compartment reactor, where a reformer and an oxidizer are directly coupled, was modelled in order to explore the potential of heat supply through methane combustion (Simakov and Sheintuch, 2008). The analysis of the composition and temperature axial and radial gradients in a membrane reforming reactor in order to identify technological and process problems has been performed by De Falco et al. (2007).
Despite, membrane modelling of steam reformers has reached a good level of development, still a number of issues regarding the suitable choice of operating conditions exist. A modelling background that will ensure rigorous optimization and control studies needs further exploitation with emphasis on model validation, effective numerical methods and acceptable computational time solutions. To this end, the aim is to develop a pseudo-homogeneous mathematical model of a fixed-bed reactor with an integrated membrane for the methane steam reforming, where both axial and radial gradients of temperature and pressure are taken into account. Furthermore, the study focuses on the effect of temperature, pressure and hydrogen removal on methane conversion and process stream composition. A comparison between methane steam reforming in a conventional and a membrane reactor is presented in order to demonstrate the advantages of the membrane reactor.

2. Reactor Geometry and Reaction Scheme

2.1 Process Description

Figure 1 shows the concept of a membrane reactor with length, L, equal to 50 cm, membrane diameter, $d_{membrane}$, equal to 12.5 mm, and reaction zone diameter, $d_{reaction\ zone}$, equal to 41.25 mm. Methane and steam are fed into the reaction zone at a molar ratio of steam to carbon (S/C) equal to 1:3, whereas reactions take place at maximum temperatures of 550 ^{o}C and maximum pressure of 10 atm over a nickel-based catalyst. Methane steam reforming and water gas shift are the two main reactions that take place leading to CO, CO_2, and H_2 as the overall products. The driving force for hydrogen removal through a permselective Pd or Pd-Ag based membrane, and thus for high hydrogen yield, as equilibrium shifts towards hydrogen production, is the hydrogen partial pressure difference between the reaction and permeation zone. Eventually, hydrogen can be carried away by the sweep gas (H_2O, N_2 or He) that flows along the permeation zone. The flexibility on heat provision can be ensured externally by utilizing molten salts from the exploitation of solar energy, combustion of biomass derived fuels or even electrical heaters. Table 1 shows the reaction scheme in methane steam reforming.

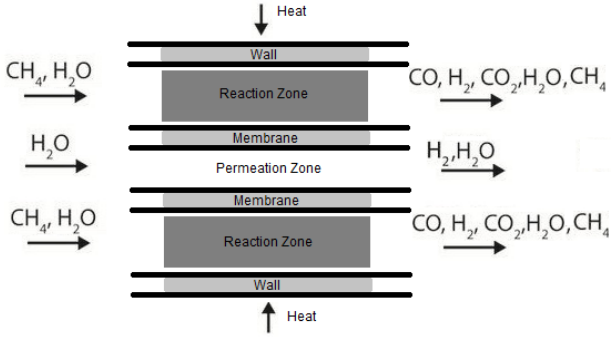

Figure 1: Membrane reactor for low temperature steam reforming

Table 1: Reaction scheme of the membrane steam reforming

Reaction		Reaction Enthalpy
Methane steam reforming (1)	$CH_4+H_2O\leftrightarrow CO+3H_2$	$\Delta H^{o}_{298} = 206\ \mathrm{kJ/mol}$
Water-Gas swift (2)	$CO+H_2O\leftrightarrow CO_2+H_2$	$\Delta H^{o}_{298} = -41\ \mathrm{kJ/mol}$
Methane steam reforming (3)	$CH_4+2H_2O\leftrightarrow CO_2+4H_2$	$\Delta H^{o}_{298} = 165\ \mathrm{kJ/mol}$

2.2 Kinetic Model

Generally, methane steam reforming involves two reversible endothermic reactions and the exothermic water-gas swift reaction. Reaction rate expressions are based on a Langmuir-Hinshelwood mechanism and are given by Xu and Froment (1989):

$$R_1 = \frac{\frac{k_1}{P_{H_2}^{2.5}}\left[P_{CH_4}P_{H_2O} - \frac{P_{H_2}^3 P_{CO}}{K_1}\right]}{DEN^2} \quad (1)$$

$$R_2 = \frac{\frac{k_2}{P_{H_2}}\left[P_{CO}P_{H_2O} - \frac{P_{H_2}P_{CO_2}}{K_2}\right]}{DEN^2} \quad (2)$$

$$R_3 = \frac{\frac{k_3}{P_{H_2}^{3.5}}\left[P_{CH_4}P_{H_2O}^2 - \frac{P_{H_2}^4 P_{CO_2}}{K_3}\right]}{DEN^2} \quad (3)$$

$$DEN = 1 + K_{CH_4}P_{CH_4} + K_{CO}P_{CO} + K_{H_2}P_{H_2} + \frac{K_{H_2O}P_{H_2O}}{P_{H_2}} \quad (4)$$

$$k_i = A_i exp\left(-\frac{E1_i}{R_g T}\right), i = CH_4, H_2O, CO, CO_2 \quad (5)$$

$$K_i = B_i exp\left(-\frac{E2_i}{R_g T}\right), i = CH_4, H_2O, CO, CO_2, 1,2,3 \quad (6)$$

Symbol R_i denotes the *i*-th reaction rate in mol/(kg cat)·s, k_i the *i*-th reaction rate coefficient in mol·atm$^{0.5}$/(kg cat)·s for *i*=1,3 and in mol/(kg cat)·s·atm for *i*=2, P_i the *i*-th component partial pressure in atm, K_i the ith reaction equilibrium constant in atm^2 for *i*=1,3 and K_j the *j*-th component adsorption constant in atm^{-1} for *j*=CH_4, CO, H_2.

3. Process Model

The two-dimensional, nonlinear and pseudo-homogeneous mathematical model consists of: a) material balances for every component both in reaction, Eq(7), and permeation zone, Eq(10), b) energy balances in the reaction zone, Eq(8), and c) momentum balances in the reaction zone, Eq(9). Hydrogen flux through the membrane is calculated by Eq(11) (Sieverts law). The assumptions that are made are: a) steady-state conditions, b) plug flow, c) ideal-gas behaviour, d) constant density, e) selectivity of the membrane towards hydrogen at 100 % (i.e. no permeation of other components), f) pseudo-homogeneous model, g) no radial gradient in permeation zone, h) no backmixing in axial direction in the reaction and permeation zones, i) constant temperature and pressure in permeation zone at their inlet values, j) no heat exchange between permeation and reaction zones and k) heat transfer in the jacket is not modelled and wall temperature is considered constant. Eq(11) provides the hydrogen flux through the membrane side:

$$\frac{\partial(uC_i)}{\partial z} = \frac{\varepsilon D_{er}}{u}\left(\frac{1}{r}\frac{\partial(uC_i)}{\partial r} + \frac{\partial^2(uC_i)}{\partial r^2}\right) + \rho_b \sum_j R_j \nu_{i,j} \quad (7)$$

$$u\rho C_p \frac{\partial T}{\partial z} = k_r\left(\frac{1}{r}\frac{\partial T}{\partial r} + \frac{\partial^2 T}{\partial r^2}\right) + \rho_b \sum_j \Delta Hr_j R_j \quad (8)$$

$$\frac{\partial P}{\partial z} = \frac{fG\mu}{\rho d_p^2}\frac{(1-\varepsilon)^2}{\varepsilon^3}, f = 150 + 1.75\frac{Re_p}{1-\varepsilon}, Re_p = \frac{G d_p}{\mu} \quad (9)$$

$$\frac{\partial\left(u_p C_{H_2 p}\right)}{\partial z} = \frac{2}{r_i}N_m, i = H_2, \frac{\partial\left(u_p C_{i_p}\right)}{\partial z} = 0, i \neq H_2 \quad (10)$$

$$N_m = \frac{Qexp\left(-\frac{15700}{R_g T_m}\right)}{d_m}\left(p_{H_{2,r}}^{0.5} - p_{H_{2,p}}^{0.5}\right) \quad (11)$$

Symbol u denotes the gas superficial velocity in m/sec, C_i the *i*-th component concentration in mol/m^3, ε the catalyst void fraction held constant at 0.85, D_{er} the effective radial diffusivity held constant at 1.238·10^{-5} m^2/s, ρ_b the catalytic bed density fixed at 1.6 kg/m^3, R_j the *j*-th reaction rate in mol/m^3·s, $n_{i,j}$ the *i*-th component moles in the *j*-th reaction in mol, ρ the gas mixture density in kg/m^3, C_p gas mixture heat capacity in kJ/mol·K, T the temperature in K, k_r the effective radial thermal conductivity held constant at 1.5 J/m·s·K, ΔHr_j the reaction heat in kJ/mol, P the pressure in atm, G the mass flow rate in kg/m^2·s, μ the mixture viscosity in kg/m·s, d_p the equivalent particle diameter fixed at 5·10^{-3} m, f the friction factor, Re_p particle Reynolds number, u_p the superficial gas velocity in the permeation zone in m/sec, C_{ip} the ith component in permeation zone in mol/m^3, r_i the membrane radius in m, N_m the hydrogen flux in mol/m^2·s,

Q denotes the pre-exponential factor of membrane permeation which is equal to 0.00022 mol/atm$^{0.5}$·m·s, d_m the membrane thickness 5·10^{-4} m, R_g the universal gas constant in kJ/mol·K, T_m the membrane temperature in K and p_{H2} the partial pressure in reaction (r) and permeation (p) zones respectively.
Boundary conditions in the reaction zone at the wall and the membrane side, and the reactor inlet are:

$$z = 0, \forall r: \quad (uC_i) = (uC_i)_{in},\ T = T_{in},\ P = P_{in},\ \left(u_p C_{i_p}\right) = 0 \tag{12}$$

$$r = r_o, \forall z: \quad \frac{\partial (uC_i)}{\partial r} = 0,\ k_r \frac{\partial T}{\partial r} = h_w (T_w - T) \tag{13}$$

$$r = r_i, \forall z: \quad \frac{\partial (uC_i)}{\partial r} = 0, i \neq H_2 \tag{14}$$

$$\frac{d_p}{Pe_m} \frac{\partial \left(uC_{H_2}\right)}{\partial r} = N_m, i = H_2$$

$$\frac{\partial T}{\partial r} = 0$$

Symbol T_{in} denotes the inlet temperature in K, P_{in} the inlet pressure in atm, h_w the thermal transmittance of the wall 150 W/m^2·K, T_w the wall temperature in K, Pe_m the Peclet number, r_o the outer diameter of the tube in m and r_i the membrane diameter in m.

4. Simulation Results

The discretization of the equations is performed via forward finite differencing in axial direction and via a central finite differencing scheme in the radial direction. The number of grid points in axial and radial direction is Nz = 230 and Nr = 5. The number of equations and variables are m = 8,531 and n = 8,519, respectively, with the remaining variables associated with the fixed inlet stream conditions. The model is validated successfully through comparison with the simulated results reported by Ipsakis et al. (2012) for a range of moderate to high pressures and temperatures.
Figures 2a and 2b show the temperature and molar fraction profiles along the normalized reactor length for operating conditions: T_{wall} = 550 °C, P_{inlet} = 10 atm, P_{mem} = 1 atm, M_{feed} = 0.29 kg/h, S/C=3. Temperature profiles are presented at three different radial positions; namely at the reaction zone near the external wall, the reaction zone centre and near the membrane in the reaction zone. At the region near the wall, temperature is higher as heat is provided through the wall. At the region near the membrane, temperature is lower due to thermal transferring, as well as, because hydrogen removal shifts the equilibrium towards the products side and since the overall reaction is endothermic temperature reduces. Methane and water consumption rate and carbon monoxide and carbon dioxide production rate are higher near the reactor entrance and lower because of composition changes but not zero because of hydrogen removal afterwards. Hydrogen molar fraction increases in the first 20 % of the reactor. Then hydrogen molar fraction decreases indicating a net positive hydrogen transfer through the membrane towards the sweep gas.

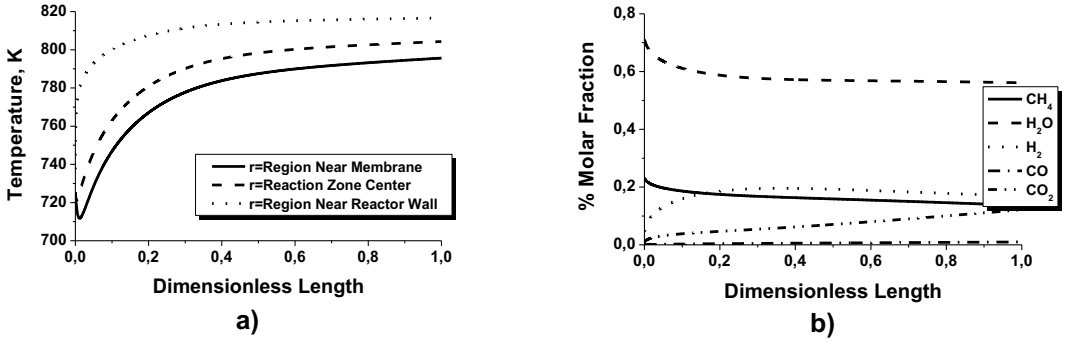

Figure 2: a) Temperature profile versus reactor length for three different radial positions, b) component mole fractions versus reactor length (averaged over radial dimension)

Tables 2 and 3 show results about the effect of the membrane (T_{inlet} = 300 °C, M_{feed} = 0.153 kg/h, P_{mem} = 1 atm and S/C = 3). Methane conversion is calculated as ($F_{CH4,in}$-$F_{CH4,out}$)/$F_{CH4,in}$ and hydrogen recovery yield as $F_{H2,out,perm}$/$F_{CH4,in}$. The value of hydrogen recovery yield can reach the value of four for ideal conversion and separation. Methane conversion is definitely higher when a membrane is used. Also, methane conversion and hydrogen recovery yield change in the membrane reactor is proportional to the hydrogen

partial pressure difference between the reaction zone and the permeation zone, the more hydrogen is removed the more the equilibrium shifts towards the products. More specifically, when pressure in the reaction zone is around 1atm, the driving force for hydrogen removal through the membrane is low and thus, methane conversion does not increase significantly since the mixture composition remains unchanged and hydrogen recovery yield is very low. At a pressure level of 5 atm, the effect of hydrogen removal is quite substantial for both 500 ^{o}C and 550 ^{o}C, whereas hydrogen recovery yield is still at low level. Hydrogen composition is higher without the membrane since hydrogen is not removed. Finally, at 10 atm the effect of the membrane is significantly more important. Methane conversion is significantly higher (up to 60.24 %) than the one obtained without the membrane. Obviously, composition of all components increases due to higher hydrogen amount removed. Hydrogen recovery yield values are even higher which means that hydrogen separation is more important at high pressure.

Table 2: Effect of the membrane at T = 500 ^{o}C for P = 1, 5, 10 atm

		Conversion %			Composition %		
T_w (^{o}C)	P_{in} (atm)	Reactor without membrane	Membrane Reactor	Hydrogen Recovery Yield	Component	Reactor without membrane	Membrane Reactor
500	1	35.05	35.72	0.01	H2	57.52%	56.83%
					CO2	13.01%	13.55%
					CO	1.94%	1.92%
					CH4	27.54%	27.70%
	5	23.95	32.82	0.57	H2	48.44%	39.81%
					CO2	11.55%	18.73%
					CO	0.87%	1.11%
					CH4	39.13%	40.36%
	10	18.86	44.74	1.35	H2	42.62%	25.08%
					CO2	10.32%	32.56%
					CO	0.58%	1.03%
					CH4	46.47%	41.33%

Table 3: Effect of the membrane at T = 550 ^{o}C for P = 1, 5, 10 atm

		Conversion %			Composition %		
T_w (^{o}C)	P_{in} (atm)	Reactor without membrane	Membrane Reactor	Hydrogen Recovery Yield	Component	Reactor without membrane	Membrane Reactor
550	1	54.26	54.65	0.02	H2	57.52%	56.83%
					CO2	13.01%	13.55%
					CO	1.94%	1.92%
					CH4	27.54%	27.70%
	5	34.44	45.5	0.79	H2	48.44%	39.81%
					CO2	11.55%	18.73%
					CO	0.87%	1.11%
					CH4	39.13%	40.36%
	10	26.65	60.24	1.93	H2	42.62%	25.08%
					CO2	10.32%	32.56%
					CO	0.58%	1.03%
					CH4	46.47%	41.33%

Figures 3a and 3b show indicative results referring to methane conversion profile and hydrogen flowrate versus reactor length. Methane conversion at three different pressures are presented (P_{inlet} = 1, 5, 10 atm, T_{wall} = 550 ^{o}C, P_{mem} = 1 atm, M_{feed} = 0.153 kg/h, *S/C*=3). Methane conversion increases faster near the entrance part of the reactor but slows downstream. This is attributed to the balance achieved between competing reaction rate changes due to hydrogen removal and species concentration variations. At P_{inlet} = 1 atm no effect due to hydrogen removal is observed. At P_{inlet} = 5 atm conversion becomes lower due to equilibrium and although methane conversion is higher than without membrane it is still lower than the one obtained when P_{inlet} = 1 atm. At P_{inlet} = 10 atm methane conversion increases slower near the entrance of the reactor than at lower pressures but its increase rate remains high due to hydrogen removal. Hydrogen flowrate at three different radial positions are presented (P_{inlet}=10 atm) in Figure 3b. At the region near the

wall of the tube, hydrogen flowrate is higher and near the membrane hydrogen flowrate is lower due to hydrogen removal. As can be seen, methane conversion reaches 60 % for the dimensions of the reactor and for the conditions under which the simulations where performed, but it seems possible to obtain even higher values with a longer reactor.

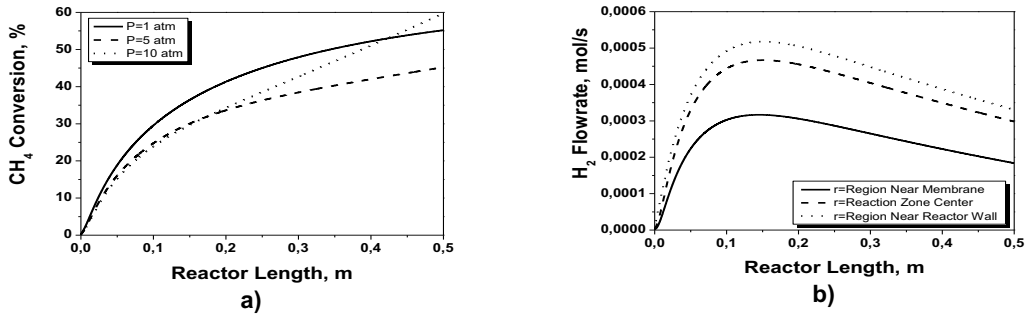

Figure 3: a) Methane conversion profile versus reactor length at three different pressures, b) hydrogen flowrate versus reactor length at three different radial positions

5. Conclusions

Methane steam reforming in a membrane reactor has been studied from a modelling point of view. An analysis about the effect of pressure, temperature and hydrogen removal through the membrane has been performed. Results suggest that high methane conversion values can be reached within a membrane reaction in significantly lower temperatures than in traditional reactors as hydrogen removal through a permselective membrane shifts equilibrium towards hydrogen production.

6. Acknowledgment

The financial support of the European Commission under the FP7 Fuel Cells and Hydrogen Joint Technology Initiative grant agreement FP7-2013-JTI-FCH-279075 is gratefully acknowledged.

References

Bientinesi M., Petarca L., 2011. H2 separation from gas mixtures through palladium membranes on metallic porous support. Chemical Engineering Transactions, 24, 763-768.

De Falco M., Barba D., Cosenza S., Iaquaniello G., Marrelli L., 2008. Reformer and membrane modules plant powered by a nuclear reactor or by a solar heated molten salts: Assessment of the design variables and production cost evaluation. International Journal of Hydrogen Energy, 33(20), 5326-5334.

De Falco M., Di Paola L., Marrelli L & Nardella P., 2007. Simulations of large-scale membrane reformers by a two-dimensional model. Chemical Engineering Journal, 128(2-3), 115-125.

De Falco M., Iaquaniello G., Marrelli L., 2009. Reformer and membrane modules plant for natural gas conversion to hydrogen:performance assessment. Chemical Engineering Transactions, Volume 17, 1407-1412. DOI: 10.3303/CET0917235.

De Falco M., Iaquaniello G., Salladini A., 2011a. Experimental tests on steam reforming of natural gas in a reformer and membrane modules, (RMM) plant). Journal of Membrane Science, 368(1-2), 264-274.

De Falco M., Marrelli L., Iaquaniello G., 2011b. Membrane reactors for hydrogen production. London, UK: Springer.

Ipsakis D., Kyriakides A., Ouzounidou M., Drakaki K., Voutetakis S., Papadopoulou S., Seferlis P. & Lemonidou A., 2012. Catalytic methane steam reforming at low temperatures with parallel hydrogen removal through an integrated Pd membrane. Panhellenic Symposium of Catalysis, paper O4, Crete, Greece (in Greek).

Simakov D.S.A., Sheintuch M., 2008. Design of a thermally balanced membrane reformer for hydrogen production. AlChE Journal, 54(10), 2735-2750.

Simakov D.S.A & Sheintuch M., 2010. Experimental optimization of an autonomous scaled-down methane membrane reformer for hydrogen generation. Industrial and Engineering Chemistry Research, 49(3), 1123-1129.

Xu J., Froment G. F., 1989. Methane steam reforming, methanation and water-gas shift: Intrinsic Kinetics. AlChE Jounral, 35(1), 88-96.